Correlations between the shifts in prompt gamma emission profiles and the changes in daily target coverage during simulated pencil beam scanning proton therapy

Lens, Eelco; Jagt, Thyrza; Hoogeman, Mischa; Schaart, Dennis

Important note
To cite this publication, please use the final published version (if applicable).
Please check the document version above.

Correlations between the shifts in prompt gamma emission profiles and the changes in daily target coverage during simulated pencil beam scanning proton therapy

Recent citations

- Imaging issues specific to hadrontherapy (proton, carbon, helium therapy and other charged particles) for radiotherapy planning, setup, dose monitoring and tissue response assessment
  J. Thariat *et al*

- An Approach for Optimizing Prompt Gamma Photon-Based Range Estimation in Proton Therapy Using Cramér–Rao Theory
  E. Lens *et al*

- Compact Method for Proton Range Verification Based on Coaxial Prompt Gamma-Ray Monitoring: A Theoretical Study
  Fernando Hueso-Gonzalez and Thomas Bortfeld
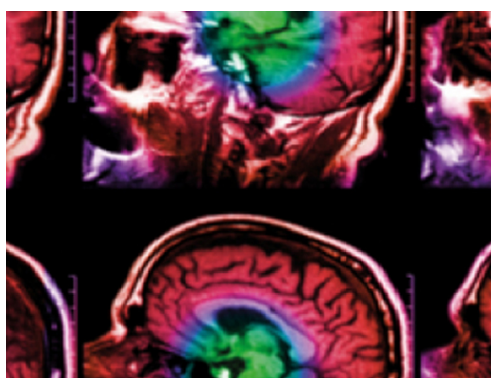
Physics in Medicine & Biology

Correlations between the shifts in prompt gamma emission profiles and the changes in daily target coverage during simulated pencil beam scanning proton therapy

Eelco Lens[1,4], Thyrza Z Jagt[2], Mischa S Hoogeman[2,3] and Dennis R Schaart[1,3]

[1] Department of Radiation Science and Technology, Delft University of Technology, Delft, The Netherlands
[2] Department of Radiation Oncology, Erasmus MC Cancer Institute, Rotterdam, The Netherlands
[3] Holland Proton Therapy Center, Delft, The Netherlands
[4] Author to whom any correspondence should be addressed.

E-mail: e.lens@tudelft.nl

Abstract

The aim of this study was to investigate the feasibility of using prompt gamma (PG) ray emission profiles to monitor changes in dose to the planning target volume (PTV) during pencil beam scanning (PBS) proton therapy as a result of day-to-day variation in patient anatomy.

For 11 prostate patients, we simulated treatment plan delivery using the patients' daily anatomy as observed in the planning CT and 7–9 control CT scans, including the detected PG profiles resulting from the 5%, 10%, and 20% most intense proton pencil beams. For each patient, we determined the changes in dosimetric parameters for the high- and low-dose PTVs between the simulations performed using the planning CT scan and the different control CT scans and correlated these to changes in the PG emission profiles.

Changes in coverage of the high- and low-dose PTV correlated most strongly with the median and mean absolute PG emission profile shifts of the 5% most intense pencil beams, respectively. With a mean Pearson correlation coefficient of -0.76 (SD: 0.17) for the high-dose PTV and of -0.60 (SD: 0.51) for the low-dose PTV.

We showed, as a proof of principle, that PG emission profiles obtained during PBS proton therapy could be used to detect changes in PTV coverage due to day-to-day anatomical variation.

Introduction

Proton therapy can be negatively affected by errors in proton range prediction and by day-to-day anatomical variations, both resulting in a variation in the Bragg peak location, this study focusses on the latter. The sensitivity of proton therapy accuracy to small daily anatomical variations, as well as the corresponding effects on the dose distribution, have been previously described (Paganetti 2012). The detection of secondary radiation exiting the patient has been proposed as a potential tool for day-to-day dose monitoring, so as to ensure patient safety and an effective treatment (Parodi *et al* 2005, Min *et al* 2006, Cambraia Lopes *et al* 2015, 2016, Krimmer *et al* 2018, Parodi and Polf 2018).

Prompt gamma (PG) rays resulting from nuclear interactions between the incoming protons and the patients' tissue can be used for proton range monitoring during treatment (Min *et al* 2006). PG emission profiles have been shown to correlate strongly with the depth-dose profile of the primary proton beam (Min *et al* 2006). Detecting changes in the location of the fall-off region of the PG emission profiles to estimate the change in proton range has been shown to be feasible in both Monte Carlo simulations as well as in *in situ* and *in vivo* measurements (Moteabbed *et al* 2011, Cambraia Lopes *et al* 2015, Richter *et al* 2016, Nenoff *et al* 2017). Different techniques have been proposed, such as using spectral or timing information (Verburg *et al* 2012, 2013, Golnik

et al 2014, Verburg and Seco 2014) or neutron background suppression by applying time-of-flight discrimination (Cambraia Lopes *et al* 2015).

PG emission profile measurements have been used in a clinical setting and in combination with patient data (Janssen *et al* 2014, Schmid *et al* 2015, Janssens *et al* 2016, Richter *et al* 2016, Xie *et al* 2017). However, information was provided on range shifts of individual pencil beams or energy layers only, not on clinically relevant dosimetric parameters, which is needed to ensure daily target coverage and to increase treatment effectiveness.

If PG emission profiles are to be used for (near) real-time dose monitoring during proton therapy, the deviation between the detected and expected PG emission profiles should be determined. In addition, a translation from the simple detection of range shifts for a set of pencil beams to the quantitative assessment of clinically relevant changes in the dose distribution should be established. To our knowledge, it has not yet been shown whether changes in PG emission profiles correlate with changes in clinically relevant dosimetric parameters such as target coverage.

The goal of this study is to investigate the feasibility of using detected PG emission profiles for the daily monitoring of dosimetric changes during pencil beam scanning (PBS) proton therapy. We used Monte Carlo to simulate dose delivery on multiple control CT scans to determine the changes in dose to target volumes and in PG emission profiles, detected outside the patient, as a result of day-to-day variation in patient anatomy. We established the correlations between dosimetric changes and changes in the PG emission profiles to determine what observables could potentially be used for day-to-day dose monitoring.

Materials and methods

Clinical dataset and treatment plans

Our dataset consisted of 11 prostate cancer patients, previously treated with conventional intensity modulated radiotherapy (IMRT) without a bladder filling protocol or rectal balloon. For each patient we had a planning CT scan and 7–9 control CT scans (supplementary table A1 (stacks.iop.org/PMB/64/085009/mmedia)), obtained during the course of treatment (99 CT scans in total). The available CT scans represented the day-to-day anatomical variations as were observed for this patient group in daily practice. These anatomical changes can result in density changes along the pencil beam path affecting the dose distribution.

For each planning CT scan, we had a structure set delineated by an experienced radiation oncologist. We generated the high-dose planning target volume (PTV_{high}; prostate + 4 mm) and the low-dose PTV (PTV_{low}; seminal vesicles + lymph nodes + 7 mm). In addition, there was the intermediate-dose PTV (PTV_{inter}), which consisted of part of the PTV_{low} that was situated in the 15 mm ring surrounding the PTV_{high} that was used to regulate the dose gradient around the PTV_{high} during plan optimization (Jagt *et al* 2017). The PTV_{inter} was excluded from the PTV_{low}, thus these two volumes did not overlap. The PTV_{high} was prescribed 74 Gy in 37 fractions of 2 Gy, the PTV_{low} and PTV_{inter} were prescribed 55 Gy but the PTV_{inter} will partially receive a higher dose since it is situated in the dose gradient surrounding the PTV_{high}. For each patient, a PBS proton treatment plan was made using the Erasmus-iCycle treatment planning system (van de Water *et al* 2013, Jagt *et al* 2017) and the dose was calculated using the 'Astroid' dose engine (Kooy *et al* 2010). This system generates Pareto-optimal plans by using a multi-criteria optimization based on constraints and objectives. All planning constraints and objectives were in accordance with the work from Jagt *et al* (2017). On average, a plan contained 1417 (range: 1247–1540) pencil beams and a total of 2.8×10^{12} to 3.6×10^{12} protons (supplementary table A1), divided over two opposing lateral fields. The plans were not robustly optimized.

Monte Carlo simulation of dose delivery and PG detection

Dose delivery using the proton therapy plans was simulated using the TOPAS (version 3.1.p1) (Geant4 10.3.p01 based) Monte Carlo code (Perl *et al* 2012) and was performed on the Dutch national computing cluster LISA (SURFsara, Amsterdam, the Netherlands). We used the TOPAS default physics list, which has been shown to compare well to lists that were proposed for proton therapy in earlier versions of Geant4 (Jarlskog and Paganetti 2008). Geant4 has been shown to overestimate PG yields, while the PG emission profile length was accurately simulated (Pinto *et al* 2016).

We extracted the treatment parameters (e.g. pencil beam energies and locations relative to the isocenter) from the treatment plans and used these to generate the initialization files required to perform the simulations. The pencil beam weights were determined by dividing the number of monitor units (MUs) per pencil beam by the number of MUs of the most intense pencil beam within that treatment plan. For each plan, the most intense pencil beam was simulated using 2.8×10^6 protons and the number of protons of the other pencil beams were scaled by the corresponding beam weight. This resulted in an approximate downscaling of the actual number of planned protons by a factor of 5000 and on average 3.3×10^5–5.3×10^5 simulated protons per pencil beam per patient. The maximum number of protons was used to evenly distribute the available calculation time over all

patients. The number of pencil beams and the number of planned and simulated protons per treatment plan are given in supplementary table A1.

For each patient, dose delivery was simulated on both the planning and control CT scans to obtain dose distributions and PG emission profiles corresponding to the anatomy represented on all CT scans. The extracted dosimetric values from the simulated planned dose distributions (i.e. treatment plans simulated on the corresponding planning CT scans) were used as reference values for each patient. This was done to negate any differences between the dose calculation engine of Erasmus-iCycle and TOPAS. The extracted values from the simulated dose distributions on the control CT scans were compared to the reference values to establish how the dose changed due to day-to-day anatomical variations.

In daily clinical practice, the patient is positioned based on a registration of the intra-prostatic markers. In this study, the isocenter of each CT, which was defined as the center of mass of the prostate, was placed at the origin of our coordinate system, mimicking perfect daily patient positioning. No positioning uncertainty of an envisioned PG emission detector was taken into account since we assumed a fixed detector position with respect to the isocenter of the treatment unit. The conversion from Hounsfield Units to proton stopping power was performed using the Schneider (stoichiometric) conversion (Schneider *et al* 2000). The used Hounsfield look-up table was not optimized for the used CT scanner and conversion uncertainties were not taken into account, but this should not influence the relative difference between the different simulations.

For each simulation, we scored the dose (i.e. dose to water) deposited within the CT volume on a 200×200 grid for each CT slice, resulting in slightly different voxel sizes per patient. However, this will not influence the results since no inter-patient comparison will be performed. All photons exiting the patient were scored on a cylindrical surface around the CT volume, coaxially to the treatment fields. For each photon, the position, direction, energy and which pencil beam generated the photon were scored. This allowed us to analyze PG emission profiles per pencil beam. The scoring cylinder encompassed the complete CT and would intersect with the patient in real life, but was used to increase the number of detected PG photons compared to using a scoring surface with an area similar to that of clinically used detectors (Cambraia Lopes *et al* 2015).

The creation of the initialization files as well as all data analysis was performed in MATLAB (The MathWorks Inc., Natick, MA, USA).

Data analysis

The simulated dose files were linearly interpolated to the same grid as the planned dose distribution. All dose distributions were evaluated on the planning CT scan of that patient, which means that all dosimetric parameters were determined for the PTVs as defined on the planning CT scan. This ensured that observed dosimetric changes were solely caused by changes in the dose distributions resulting from density changes observed along the pencil beam path. If the PTV, as delineated on the control CT scan, would be used, changes in dose could also be due to delineation variations and this would then not be observed in the PG emission profiles. The aim of this study was to show the feasibility of using PG emission profiles to determine changes in volumetric dosimetric parameters.

For each dose distribution, we created dose volume histograms (DVHs) for the different PTVs. We then calculated the mean dose (D_{mean}), median dose (D_{median}), the maximum dose received by $\geqslant 2\%$ of the volume ($D_{2\%}$), the minimum dose received by $\geqslant 98\%$ of the volume ($D_{98\%}$), and the volume percentage receiving $\geqslant 95\%$ of the prescribed dose ($V_{95\%}$).

To determine the PG emission profiles, we discriminated the scored photons based on energy ($\geqslant 1$ MeV) and angle of incidence ($87° \leqslant \theta \leqslant 93°$), as were used in other studies as well (Biegun *et al* 2012, Janssen *et al* 2014). The latter was done to select photons that were emitted close to perpendicular to the treatment beam, simulating a simple multi-slit collimator. We tallied the photons within 4 mm wide spatial bins resembling the pixel size of a realistic scintillation detector (Cambraia Lopes *et al* 2015). Next, we selected the PG emission profiles corresponding to the 5%, 10% and 20% most intense pencil beams (i.e. highest number of protons) per plan, regardless of the pencil beam locations or proton energy. To reduce noise, each profile was filtered using a third-order median filter. The total number of protons in the selected pencil beams corresponded to approximately 18%, 30% and 49% of the total number of protons in the treatment plans, respectively. The total numbers of simulated protons in the selected pencil beams and the total number of PG photons used for analysis are given in supplementary table A2.

For each PG emission profile, we calculated five parameters that could each be used to compare the profiles from the simulated planned dose to those from the simulations on the control CT scans. For the first and second parameters, we automatically selected the point closest to the 50%-point of the falloff region of the PG profile. Next, we selected ten points in both direction and these 21 points were considered as the falloff region of the PG profile. We fitted a sigmoid function to the falloff region and used the 50%-point of the sigmoid curve (X_{50}) as a measure for the falloff location of the profile (figure 1) (Janssen *et al* 2014). This point is known to correlate strongly with the Bragg peak location of the corresponding pencil beam (Min *et al* 2006). For each analyzed pencil beam, we determined the difference as well as the absolute difference between the X_{50} of the simulation on the
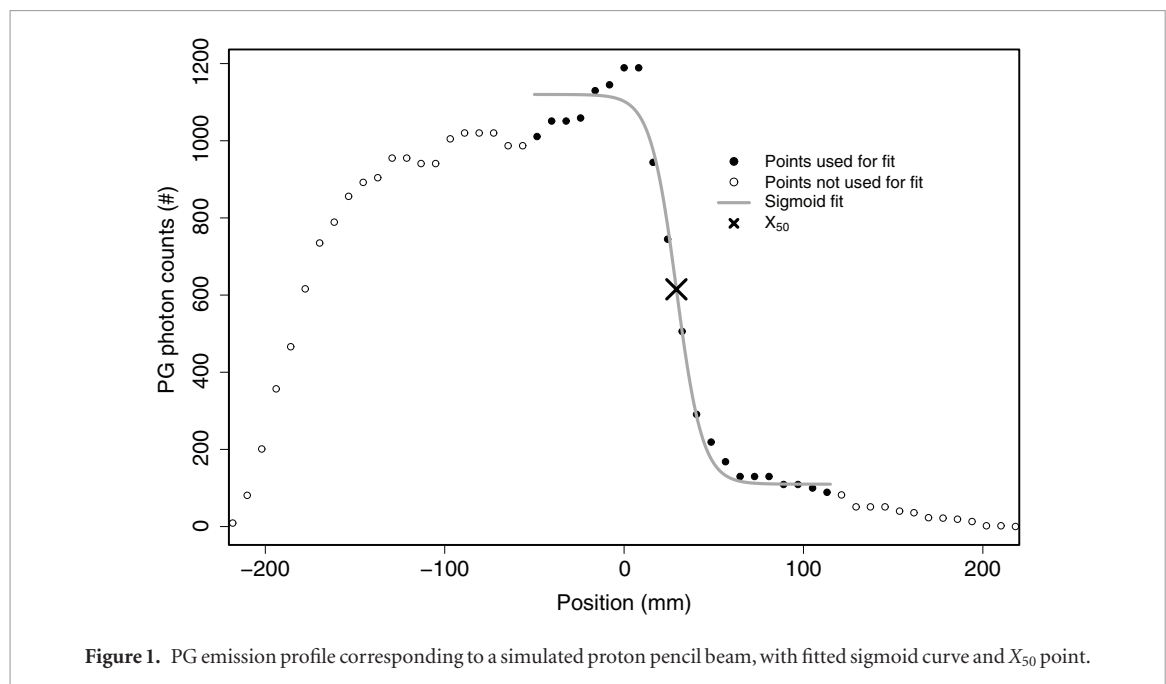
Figure 1. PG emission profile corresponding to a simulated proton pencil beam, with fitted sigmoid curve and X_{50} point.

planning CT scan and the X_{50} of that same pencil beam when simulated on the control CT scan (i.e. ΔX_{50} and $|\Delta X_{50}|$). For the third parameter, we summed the squared differences of the falloff region between the PG profiles belonging to the same pencil beams of the different simulations (i.e. local summed-squared differences). For the fourth and fifth parameters, we summed the squared differences and the chi-squared differences over the entire profiles (i.e. overall summed-squared and chi-squared differences). As a result, for each simulation on a control CT scan, we had three distributions of values for each of the five parameters, namely for the 5%, 10% and 20% most intense pencil beams, respectively.

To investigate the feasibility of using these distributions for dose monitoring during treatment, we calculated the mean, median, and standard deviation (SD) of each distribution and determined, per patient, the Pearson correlation coefficients (r) between these values and the calculated dosimetric parameters. The Pearson correlation coefficient is a measure of the linear correlation strength between two variables and can range from $-1 \leqslant r \leqslant 1$, where a negative value of r stands for a negative correlation and a positive value for a positive correlation. Small errors in the sigmoid fits to the fall-off regions of the PG emission profiles due to low counting statistics will only have a minor influence on the results since for each simulation we averaged over ± 70 to ± 280 pencil beams, depending on whether 5%, 10% or 20% of the pencil beams was used.
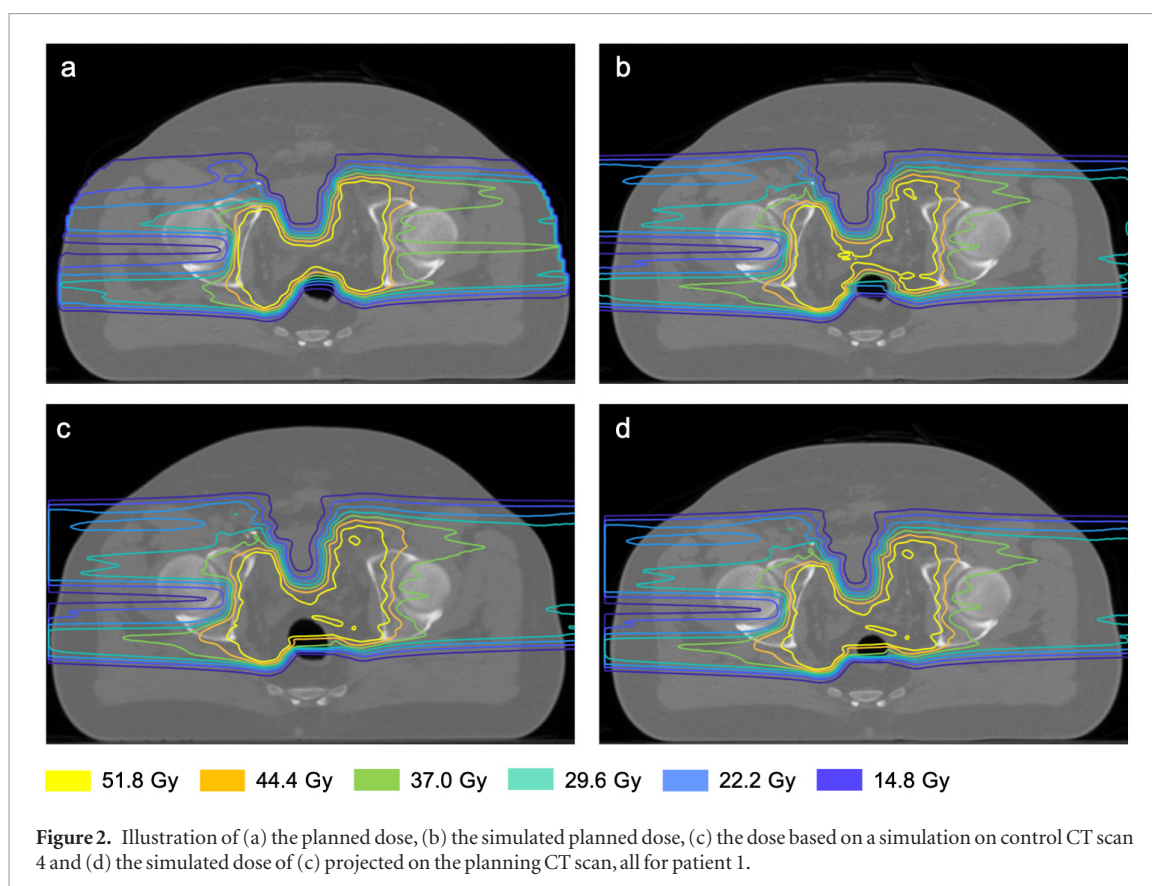
No comparison was made between the five parameters used to determine the PG profile shifts and the individual Bragg-peak shifts since we did not score the dose per pencil beam. We were only interested in the PG profile shifts of a subset of pencil beams and the clinically relevant dosimetric changes.

Results

Figure 2 exemplarily shows the planned dose distribution, the simulated planned dose distribution, the dose distribution obtained from the simulation on control CT scan 4, and the same dose distribution shown on the planning CT scan, all for patient 1. The situations shown in figures 2(a), (b) and (d) were used for the calculation of the dosimetric parameters, the situation in figure 2(c) is purely illustrative of what was simulated. In addition, figure 3 shows the DVHs of patient 4, illustrating the agreement between the planned and simulated planned dose for this patient.

Correlations between changes in PG emission profiles and in dosimetric parameters
Figure 4 shows the ΔX_{50} and $|\Delta X_{50}|$ distributions when using the 5% most intense pencil beams for patient 4. For this particular patient, the Pearson correlation coefficients between the change in $V_{95\%}$ of the PTV$_{high}$, PTV$_{inter}$ and PTV$_{low}$ (figure 3) and the mean ΔX_{50} (figure 4(a)) were 0.29, 0.10 and 0.20, respectively. When using the mean $|\Delta X_{50}|$ (figure 4(b)), the coefficients were -0.97, -0.81, -0.99. In general, stronger correlations were observed when using the absolute shifts of the PG profiles (i.e. disregarding whether a profile shifts in one direction or the other). The calculated correlation coefficients over all patients when using $|\Delta X_{50}|$ are illustrated in figure 5 in the form of box plots. The strongest correlations were observed for the $V_{95\%}$ of the PTV$_{high}$ and PTV$_{low}$. This is because the deposited dose was optimized to be conformal to and uniform within these PTVs. Therefore, a disturbance in dose compromises this conformality or could create cold-spots, decreasing the $V_{95\%}$. The PTV$_{inter}$

| | 51.8 Gy | | 44.4 Gy | | 37.0 Gy | | 29.6 Gy | | 22.2 Gy | | 14.8 Gy |

Figure 2. Illustration of (a) the planned dose, (b) the simulated planned dose, (c) the dose based on a simulation on control CT scan 4 and (d) the simulated dose of (c) projected on the planning CT scan, all for patient 1.

is positioned completely in the dose gradient from 74 Gy to 55 Gy, thus receiving a non-uniform dose higher than the prescribed 55 Gy. Therefore, the $V_{95\%}$ is less sensitive to disturbances, hence the weak correlations. In general, the strongest correlations were observed when using the 5% most intense pencil beams.

Figure 6 shows the linear fits used to calculate the correlation coefficients r and the corresponding p-values between the $V_{95\%}$ of the PTV_{high} and the median $|\Delta X_{50}|$ when using the 5% most intense pencil beams, for all patients. We observed strong correlations in most patients, but the relation between the two parameters was highly variable between patients.

Using either the $|\Delta X_{50}|$, local summed-squared differences, overall summed-squared differences or the overall summed chi-squared differences yielded similar results, but the strongest correlations were observed when using the $|\Delta X_{50}|$. This section therefore focused on the $|\Delta X_{50}|$ distributions; the other results are shortly discussed in the supplementary materials (supplementary figures A1–A4).

Discussion

This study is the first to correlate the day-to-day changes in PG emission profiles with the day-to-day volumetric dosimetric changes of the PTVs for fractionated PBS proton therapy of prostate cancer patients. The observed correlations indicate that PG emission profiles could be used to detect daily volumetric dosimetric changes.

The strength of the observed correlations and the relations between the changes in dose and PG emission profiles varied greatly. For example, weaker correlations were observed for the mean, median and max dose to the PTV_{high} and PTV_{low}. This was to be expected since a shift of a subset of the pencil beams within the volume does not necessarily change these parameters, while it does shift the PG emission profiles. Therefore, we did not report on the exact relations between the parameters extracted from the PG profiles and the dosimetric parameters. The large variation in correlation strength indicates that the calculated relations, which could be established through linear fitting, would vary greatly in predictive value and would have little added value. In addition, population-based relations could also not be determined due to the large variation between patients. This study was also limited by statistics in terms of the number of incident protons that were simulated and this inhibited using all pencil beams for analysis because many would simply have a too low number of detected PG photons. The aim of the current work was to establish, as a proof of principle, that correlations between the changes in PG emission profiles and in dosimetric parameters exist.

The simulated target coverage was considerably lower compared to what was planned and would not be clinically acceptable. This was due to the difference in dose calculation technique and an imperfect translation of the
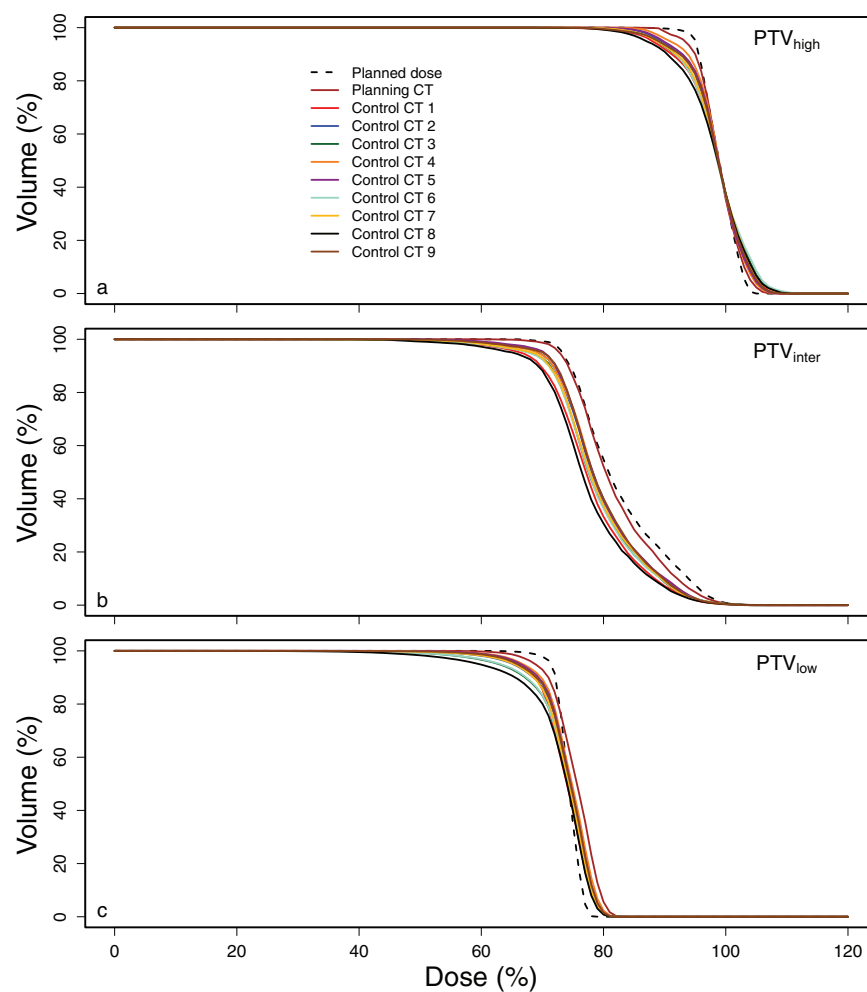
Figure 3. Dose volume histograms of (a) the high-dose PTV (PTV$_{high}$), (b) the intermediate-dose PTV (PTV$_{inter}$) and (c) the low-dose PTV (PTV$_{low}$) for all available dose distributions of patient 4.
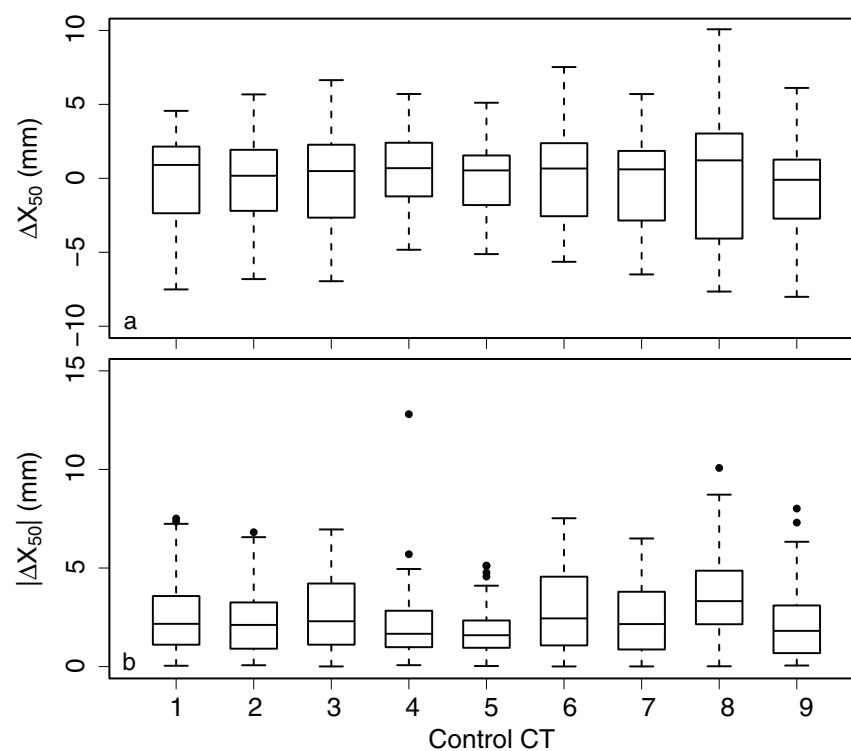

Figure 4. The (a) ΔX_{50} and (b) $|\Delta X_{50}|$ distributions when using the 5% most intense pencil beams for patient 4.
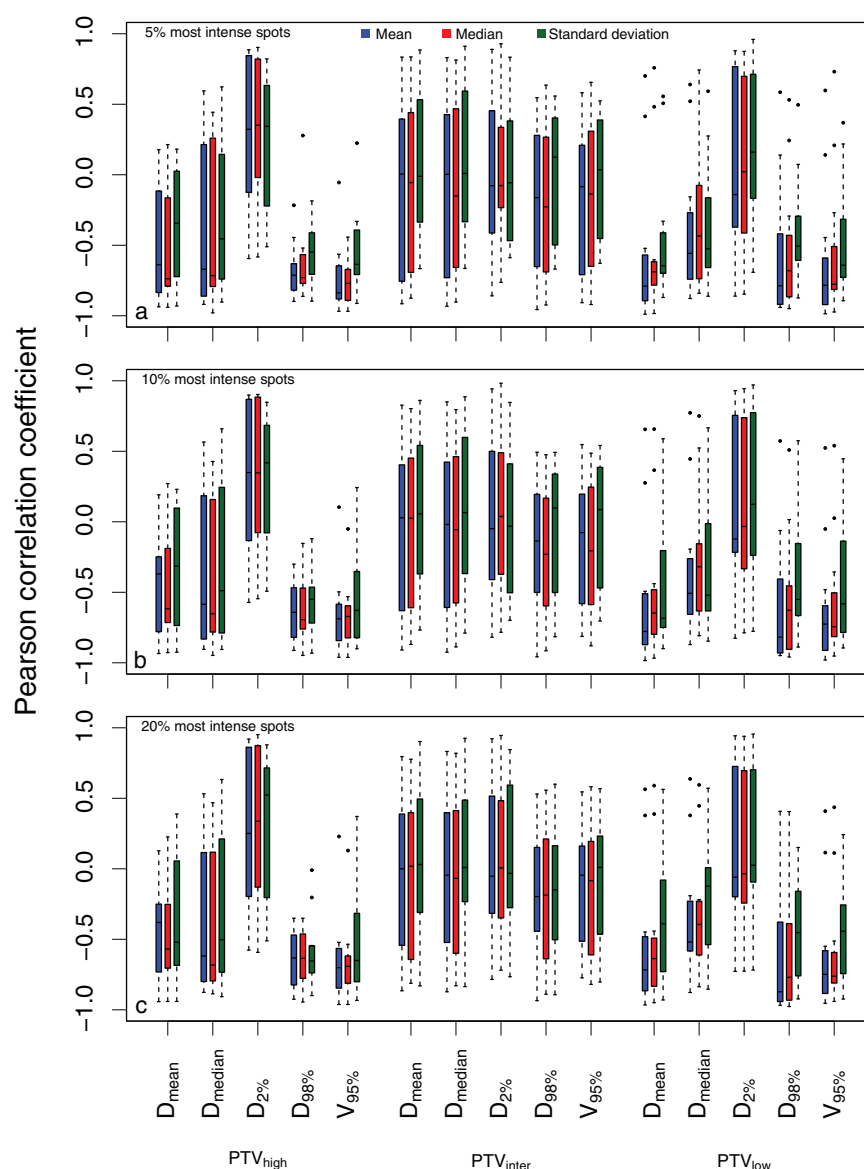
Figure 5. Distributions of Pearson correlation coefficients between the mean, median and standard deviation (color coded) of the $|\Delta X_{50}|$ distributions and the dosimetric parameters when using the (a) 5%, (b) 10% or (c) 20% most intense pencil beams.

plan parameters (e.g. exact angles of incidence), compromising the target coverage when compared to a fully optimized dose distribution. However, this did not influence the result since we only analyzed the relative differences.

If the proposed technique is to be used for dose monitoring in clinical practice, a set of reference PG emission profiles should be determined before the first treatment fraction, which could be done through Monte Carlo simulations. However, the full detector system (e.g. collimator and detector characteristics) should be considered in the predictive model. It would also be possible to determine the reference profiles from measurements during the first treatment fraction, but in this case no dose monitoring could be done during this fraction. In addition, if there is a large difference in patient anatomy during this first fraction, all subsequent fractions might be classified as incorrect.

The presented approach for dose monitoring using PG is not suitable for treatment plans that are re-optimized on a daily basis because there are no reference profiles to which the profiles of that day can be compared. It could e.g. be possible to calculate the new reference PG profiles from a re-optimized dose distribution by using a filtering approach similar to the approach described by Parodi *et al* for dose monitoring using positron emission tomography techniques (Parodi and Bortfeld 2006).

Only small differences were observed between the result when using the 5%, 10% or 20% most intense pencil beams. It thus appears that relatively little information is added when increasing the number of pencil beams used for analysis when using the current pencil beam selection method (i.e. based on intensity). Other pencil beam selection methods (e.g. based on their contribution to specific dosimetric parameters) could benefit from
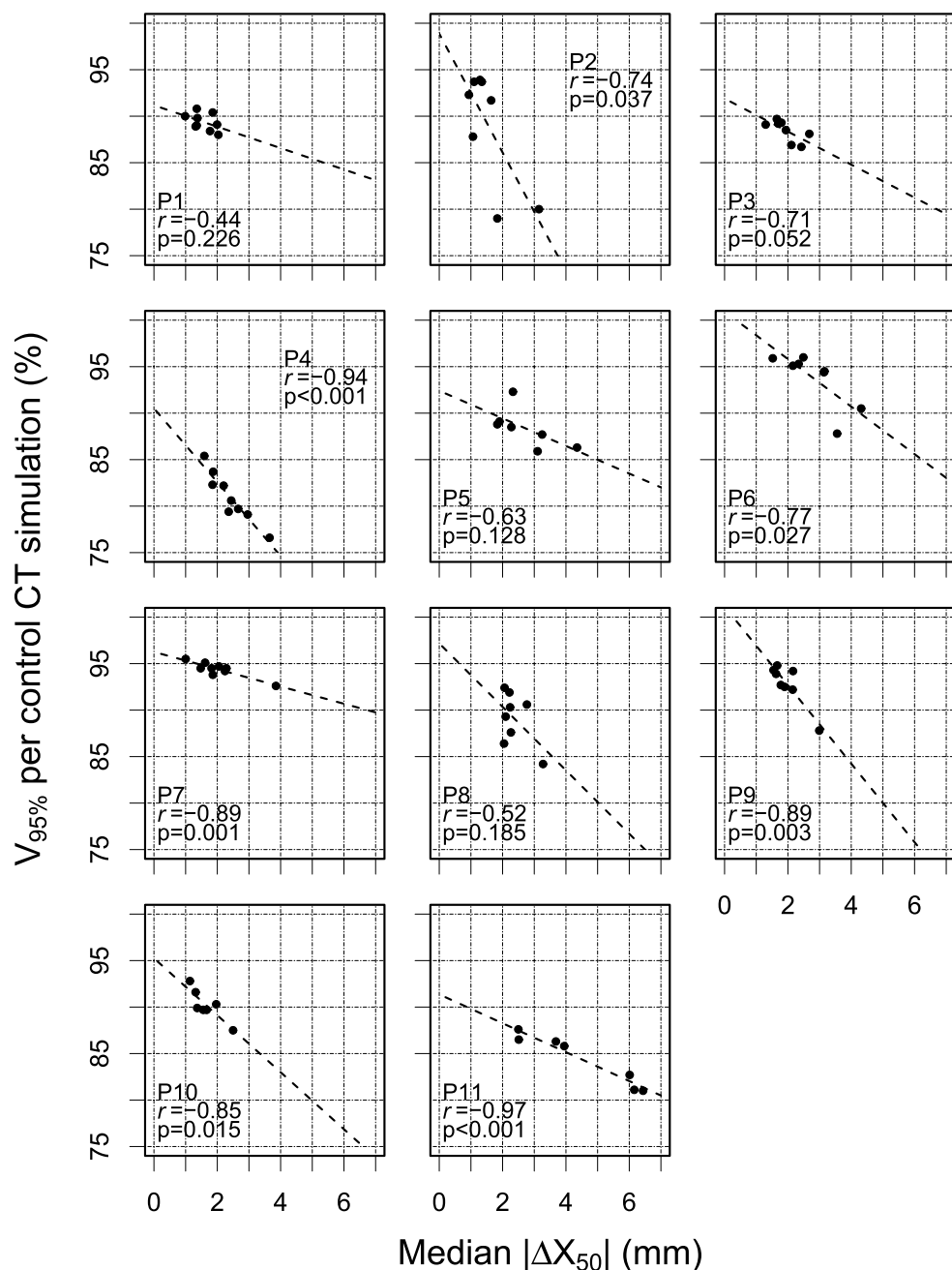
Figure 6. Scatter plots of the target coverage of the high dose PTV ($V_{95\%}$) and the median $|\Delta X_{50}|$ when using the 5% most intense pencil beams for all patients (one patient per panel). Linear fits were performed to calculate the Pearson correlation coefficient (r) and corresponding p-values.

using a greater number of pencil beams for analysis. Other factors that can have an even greater effect on the performance of the proposed method are the background signal caused by neutrons and including a realistic detector efficiency.

The pencil beam selection method that was used in this study was purely based on achieving the best counting statistics for the PG emission profiles. Since the 20% most intense pencil beams automatically included the 10% most intense pencil beams and again this included the 5% most intense pencil beams, the results from these three selections were correlated. Future research should focus on deriving parameters from the detected PG signals that have better specificity. For example, by selecting pencil beams that specifically contribute to the dose to a selected structure rather than the most intense beams, and using these pencil beams to determine dosimetric changes for that structure. Then, it might be possible to determine the exact relations between the PG emission profile shifts and the dosimetric parameters and to determine exact threshold values and action levels that can be used for dose monitoring in daily practice. This was not possible in the current work because of a too low number of simulated protons per pencil beam and a change in pencil beam selection could result in performing the

analysis with PG emission profiles that had a poor contrast-to-noise ratio. In addition, devising methods to select pencil beams that contribute to specific dosimetric parameters was outside the scope of this study.

This study has a number of known limitations such as: relatively low counting statistics, the use of a perfect and cylindrical detector surface, the rejection of neutrons at the detector surface, using only the PTV on the planning CT to calculate the dosimetric parameters, and not considering positioning uncertainties. Despite these limitations, the obtained results are a next step in the advancement of PG treatment monitoring research. The presented data shows that there is a correlation between the shifts of a set of PG emission profiles and the change in volumetric dosimetric parameters. This is a first step in the clinical translation of the detection of range shifts of individual pencil beams to changes in clinically relevant dosimetric parameters.

Conclusion

It appears feasible to use PG ray emission profiles, obtained during PBS proton therapy, to detect dosimetric changes of the PTVs resulting from day-to-day anatomical variations. Changes in PTV coverage correlate with changes in PG emission profiles, but more research is needed to establish the exact relation between the changes in PG emission profiles and in dosimetric parameters. PG based treatment monitoring could then be used to obtain real-time quantitative information on the dosimetric quality in a non-invasive manner.

Acknowledgments and conflict of interests

ORCID iDs

Thyrza Z Jagt ● https://orcid.org/0000-0001-9196-8559
Dennis R Schaart ● https://orcid.org/0000-0002-3199-5608

References

Biegun A K *et al* 2012 Time-of-flight neutron rejection to improve prompt gamma imaging for proton range verification: a simulation study *Phys. Med. Biol.* **57** 6429–44

Cambraia Lopes P, Bauer J, Salomon A, Rinaldi I, Tabacchini V, Tessonnier T, Crespo P, Parodi K and Schaart D R 2016 First *in situ* TOF-PET study using digital photon counters for proton range verification *Phys. Med. Biol.* **61** 6203–30

Cambraia Lopes P *et al* 2015 Time-resolved imaging of prompt-gamma rays for proton range verification using a knife-edge slit camera based on digital photon counters *Phys. Med. Biol.* **60** 6063–85

Golnik C *et al* 2014 Range assessment in particle therapy based on prompt γ-ray timing measurements *Phys. Med. Biol.* **59** 5399–422

Jagt T, Breedveld S, van de Water S, Heijmen B and Hoogeman M 2017 Near real-time automated dose restoration in IMPT to compensate for daily tissue density variations in prostate cancer *Phys. Med. Biol.* **62** 4254–72

Janssen F, Landry G, Cambraia Lopes P, Dedes G, Smeets J, Schaart D R, Parodi K and Verhaegen F 2014 Factors influencing the accuracy of beam range estimation in proton therapy using prompt gamma emission. *Phys. Med. Biol.* **59** 4427–41

Janssens G, Smeets J, Vander Stappen F, Prieels D, Clementel E, Hotoiu E L and Sterpin E 2016 Sensitivity study of prompt gamma imaging of scanned beam proton therapy in heterogeneous anatomies *Radiother. Oncol.* **118** 562–7

Jarlskog C Z and Paganetti H 2008 Physics settings for using the Geant4 toolkit in proton therapy *IEEE Trans. Nucl. Sci.* **55** 1018–25

Kooy H M *et al* 2010 A case study in proton pencil-beam scanning delivery *Int. J. Radiat. Oncol.* **76** 624–30

Krimmer J, Dauvergne D, Létang J M and Testa É 2018 Prompt-gamma monitoring in hadrontherapy: a review *Nucl. Instrum. Methods Phys. Res.* A **878** 58–73

Min C H, Kim C H, Youn M Y and Kim J W 2006 Prompt gamma measurements for locating the dose falloff region in the proton therapy *Appl. Phys. Lett.* **89** 183517

Moteabbed M, Espana S, Paganetti H, España S and Paganetti H 2011 Monte Carlo patient study on the comparison of prompt gamma and PET imaging for range verification in proton therapy *Phys. Med. Biol.* **56** 1063–82

Nenoff L, Priegnitz M, Janssens G, Petzoldt J, Wohlfahrt P, Trezza A, Smeets J, Pausch G and Richter C 2017 Sensitivity of a prompt-gamma slit-camera to detect range shifts for proton treatment verification *Radiother. Oncol.* **125** 534–40

Paganetti H 2012 Range uncertainties in proton therapy and the role of Monte Carlo simulations *Phys. Med. Biol.* **57** R99–117

Parodi K and Bortfeld T 2006 A filtering approach based on Gaussian-powerlaw convolutions for local PET verification of proton radiotherapy. *Phys. Med. Biol.* **51** 1991–2009

Parodi K and Polf J C 2018 *In vivo* range verification in particle therapy *Med. Phys.* **45** e1036–50

Parodi K, Pönisch F and Enghardt W 2005 Experimental study on the feasibility of in-beam PET for accurate monitoring of proton therapy *IEEE Trans. Nucl. Sci.* **52** 778–86

Perl J, Shin J, Schümann J, Faddegon B and Paganetti H 2012 TOPAS: an innovative proton Monte Carlo platform for research and clinical applications *Med. Phys.* **39** 6818–37

Pinto M, Dauvergne D, Freud N, Krimmer J, Létang J M and Testa E 2016 Assessment of Geant4 prompt-gamma emission yields in the context of proton therapy monitoring *Front. Oncol.* **6** 10

Richter C *et al* 2016 First clinical application of a prompt gamma based *in vivo* proton range verification system *Radiother. Oncol.* **118** 232–7

Schmid S, Landry G, Thieke C, Verhaegen F, Ganswindt U, Belka C, Parodi K and Dedes G 2015 Monte Carlo study on the sensitivity of prompt gamma imaging to proton range variations due to interfractional changes in prostate cancer patients *Phys. Med. Biol.* **60** 9329–47

Schneider W, Bortfeld T and Schlegel W 2000 Correlation between CT numbers and tissue parameters needed for Monte Carlo simulations of clinical dose distributions *Phys. Med. Biol.* **45** 459–78

Verburg J M, Riley K, Bortfeld T and Seco J 2013 Energy- and time-resolved detection of prompt gamma-rays for proton range verification. *Phys. Med. Biol.* **58** L37–49

Verburg J M and Seco J 2014 Proton range verification through prompt gamma-ray spectroscopy *Phys. Med. Biol.* **59** 7089–106

Verburg J M, Shih H A and Seco J 2012 Simulation of prompt gamma-ray emission during proton radiotherapy *Phys. Med. Biol.* **57** 5459–72

van de Water S, Kraan A C, Breedveld S, Schillemans W, Teguh D N, Kooy H M, Madden T M, Heijmen B J M and Hoogeman M S 2013 Improved efficiency of multi-criteria IMPT treatment planning using iterative resampling of randomly placed pencil beams. *Phys. Med. Biol.* **58** 6969–83

Xie Y *et al* 2017 Prompt gamma imaging for *in vivo* range verification of pencil beam scanning proton therapy *Int. J. Radiat. Oncol.* **99** 210–8